Aerodynamic Data Modelling and Fidelity Definition for Multifidelity Data Fusion

Mehdi Anhichem and Sebastian Timme
m.anhichem@liverpool.ac.uk

University of Liverpool
Liverpool
United Kingdom

Jony Castagna

UKRI-STFC Hartree Centre
Warrington
United Kingdom

Andrew J. Peace and Moira Maina

Aircraft Research Association Ltd
Bedford
United Kingdom

ABSTRACT

Aerodynamic data required in aircraft high-value design and performance analysis are mainly acquired through wind tunnel testing and numerical analysis. Data acquisition can be expensive and is subject to multiple sources of uncertainty. Previously, the multifidelity data fusion framework introduced by Lam, Allaire and Willcox (2015) has been adapted to enable its application to large and high-dimensional datasets involved in surface flow analysis of a large aircraft wing model. Pressure coefficient distributions on the upper surface of the wing from static pressure tapping and time-averaged dynamic pressure sensitive paint as well as complementary numerical simulations were exploited. The data fusion approach relies on the construction of intermediate surrogate models for all information sources with Gaussian process regression and fusion of the latter using a variance-weighted combination. The data fusion does not consider an absolute hierarchy in terms of accuracy between the information sources. The confidence in an information source over the design space is defined through a fidelity function tailored to each intermediate model. The work presented herein focuses on improving the intermediate model design through an adaptive choice of the covariance function and on defining a fidelity function for each information source that is grounded in practical and physical considerations.

.

1.0 Introduction

Aerodynamic data are crucial for the design and development of an aircraft and the analysis of its performance. Physical flight and wind tunnel testing and computational fluid dynamics (CFD) simulations are routinely carried out to understand the aircraft aerodynamic characteristics for different flight conditions to ensure its safe operation within its nominal flight envelope. These investigations are typically carried out to examine the forces and moments and/or the pressure distribution exerted on its surface. Deterministic numerical simulations have benefited from the ever-increasing computing power and advances in modern CFD codes to become a must in aerodynamics. However, different types of uncertainties, often associated with physical modelling approximations as well as discretisation and iterative errors, prevent numerical methods from being fully trusted when dealing with complex configurations and phenomena. To complement CFD results and to make sure the physics involved especially in edge-of-the-envelope aerodynamic flows is understood, it is essential to carry out physical wind tunnel experiments. Wind tunnel testing can be expensive and, just like numerical analysis, is subject to multiple sources of uncertainty.

Multifidelity data fusion aims to leverage information from the different aerodynamic data sources to provide a merged, robust and reliable surrogate model. Historically, methodologies based on multiple sources of varying fidelity used to a large extent a method called kriging[1], also known as Gaussian process regression. The most common incarnation when applying Gaussian processes in a data-fusion context is hierarchical kriging, often called co-kriging. Co-kriging is a multifidelity methodology that combines data from two or more models to train a single Gaussian process surrogate model[2,3,4]. For instance, these ideas were applied within the Schur complement eigenvalue framework to study transonic flutter instability while looking into aerodynamic models of varying fidelity[5]. A kriging-based function was also used to correct low-fidelity models with sparse high-fidelity data from an experimental design to study wing optimisation[6]. More recently, other popular data fusion methods involve a dimensionality reduction technique, called proper orthogonal decomposition, for multifidelity surrogate modelling of velocity or pressure fields[7,8,9].

This paper follows the work carried out in Anhichem et al.[10] where a non-hierarchical multifidelity framework previously discussed in Lam et al.[11] and Feldstein et al.[12] was revisited. The choice of this framework is motivated by its use of Gaussian processes, as it is a flexible tool for modelling complex, multidimensional surfaces that accounts for the correlation of the data in the design space while providing a measure of confidence in their prediction[13]. In addition, it is non-hierarchical; each information source is considered independently of the others and the fidelity in the model hierarchy varies over the input space. In contrast, most data fusion approaches available in the literature define a fixed hierarchical relationship between information sources which is not always appropriate. The chosen approach is composed of three main ingredients; (i) the intermediate surrogate models obtained from Gaussian process regression on each information source, (ii) the definition of fidelity functions over the input space for each information source and (iii) the fidelity-weighted combination of all intermediate models. It allows the associated framework to be flexible on the number of information sources and to benefit from each model's strengths. A limitation in the choice of this framework was associated with the prohibitive com-

putational cost of Gaussian process regression for sources with many thousand data points. Indeed, its associated cubic complexity and quadratic storage requirements restricts its application to relatively small data sets such as information on forces or sparse pressure data over the design space. In Anhichem et al.[10], a method based on stochastic variational inference developed in Hensman et al.[14] has been adopted alongside the use of graphics processing unit architecture to enable the application of the data fusion framework on large data sets and therefore the application to aircraft wing pressure distributions. To advance the application of the data fusion framework, herein we focus on two aspects; the modelling of an individual information source using Gaussian process regression and the definition of the fidelity function over the design space. The first aspect addresses the design of a Gaussian process model through its covariance function that is tailored to the structure contained in the aerodynamic data. A procedure for automatic model search is explored to improve the construction of intermediate models[15,16,17]. For the second aspect, we reflect on the fidelity function that must be grounded in practical and physical considerations.

Section 2 describes the different elements forming the multifidelity data fusion approach. The RBC12 half wing-fuselage configuration[18] and the data sources considered and data sets prepared for the study are introduced in Section 3. Section 4 presents the results of an application on a one-dimensional chordwise pressure distribution. Fidelity function definitions are given in Section 5 and used to apply the multifidelity data fusion framework on a four-dimensional input space.

2.0 Multifidelity Surrogate based on Gaussian Processes

2.1 Gaussian process regression

Gaussian processes[13] represent distributions over functions written as $f : \mathbf{x} \in \mathcal{D} \longmapsto f(\mathbf{x}) \in \mathbb{R}$ which associate an input vector $\mathbf{x} \in \mathcal{D}$ on the design space $\mathcal{D} \subseteq \mathbb{R}^d$ of dimension d with a scalar quantity. Noisy observations are often considered and written as $y(\mathbf{x}) = f(\mathbf{x}) + \varepsilon$ with the noise being an independent identically distributed Gaussian variable ε with zero mean and variance τ^2. Let $\mathbf{X} = [\mathbf{x}_1 \ \mathbf{x}_2 \ ... \ \mathbf{x}_N]$ be the matrix of N training points $\mathbf{x}_j \in \mathcal{D}$ and $\mathbf{f} = f(\mathbf{X}) = [f_1, f_2, ..., f_N]^\top$, the latent variable vector containing the values $f_j = f(\mathbf{x}_j)$. The observable variable vector is defined in the same way by $\mathbf{y} = y(\mathbf{X}) = [y_1, y_2, ..., y_N]^\top$. The main idea behind Gaussian processes is that the values of $\mathbf{y}$ are jointly Gaussian with mean $m(\mathbf{X})$ and covariance $k(\mathbf{X}, \mathbf{X})$ where m is the mean function and k is the covariance function. The notations $m(\mathbf{X})$ and $k(\mathbf{X}, \mathbf{X})$ generalise the component-wise evaluation of $\mathbf{X}$ by m and k, e.g. $m(\mathbf{X}) = [m(\mathbf{x}_1) \ m(\mathbf{x}_2) \ ... \ m(\mathbf{x}_N)]$.

A Gaussian process can be characterised and written as $\mathcal{GP}(m(\mathbf{x}), k(\mathbf{x}, \mathbf{x}'))$[13]. Since it holds for any set on the design space, it includes the set containing the training points $\mathbf{X}$ and a test point $\mathbf{x}^*$. Then, $f(\mathbf{x}^*)$ can be inferred by manipulating the joint Gaussian distribution. With additional test points, the Gaussian process prior, $p(\mathbf{y}, \mathbf{f}^*)$, can be written as a joint normal distribution over the random variable vectors $\mathbf{y}$ and $\mathbf{f}^* = f(\mathbf{X}^*)$ where $\mathbf{X}^*$ represents the matrix of testing points in $\mathcal{D}$,

$$p(\mathbf{y}, \mathbf{f}^*) = \mathcal{N}\left(\begin{bmatrix} m(\mathbf{X}) \\ m(\mathbf{X}^*) \end{bmatrix}, \begin{bmatrix} k(\mathbf{X}, \mathbf{X}) + \tau^2 \mathbf{I} & k(\mathbf{X}, \mathbf{X}^*) \\ k(\mathbf{X}, \mathbf{X}^*)^\top & k(\mathbf{X}^*, \mathbf{X}^*) \end{bmatrix} \right) \tag{1}$$

To make predictions of the function outputs, $f(\mathbf{X}^*) = \mathbf{f}^*$, the posterior distribution $p(\mathbf{f}^*|\mathbf{X}^*, \mathbf{X}, \mathbf{y})$ can be derived by applying the multivariate Gaussian conditional rule which gives $p(\mathbf{f}^*|\mathbf{X}^*, \mathbf{X}, \mathbf{y}) = \mathcal{N}(\mathbf{f}^*|\mu_{GP}(\mathbf{X}^*), \sigma_{GP}(\mathbf{X}^*))$ with posterior mean $\mu_{GP}(\mathbf{x})$ and posterior standard deviation $\sigma_{GP}(\mathbf{x})$ defined as

$$\mu_{GP}(\mathbf{X}^*) = m(\mathbf{X}^*) + k(\mathbf{X}, \mathbf{X}^*)^\top \left[k(\mathbf{X}, \mathbf{X}) + \tau^2 \mathbf{I} \right]^{-1} \left(\mathbf{y} - m(\mathbf{X}) \right) \tag{2}$$

$$\sigma_{GP}(\mathbf{X}^*) = k(\mathbf{X}^*, \mathbf{X}^*) - k(\mathbf{X}, \mathbf{X}^*)^\top \left[k(\mathbf{X}, \mathbf{X}) + \tau^2 \mathbf{I} \right]^{-1} k(\mathbf{X}, \mathbf{X}^*) \tag{3}$$

The standard deviation, σ_{GP}, quantifies the uncertainty arising from the approximation process and corresponds to the uncertainty in the model prediction away from a training point. The posterior distribution strongly depends on the formulation used for $m(\mathbf{x})$ and $k(\mathbf{x}, \mathbf{x}')$. Whereas the mean function is commonly assumed to be zero on the design space, $m(\mathbf{x}) = 0$, the covariance function incorporates the function's structure available under the Gaussian process prior. In other words, it determines the properties of the obtained Gaussian process model.

A popular choice for the covariance function is the squared-exponential,

$$k_{SE}(\mathbf{x}, \mathbf{x}') = \sigma^2 \exp \left(-\sum_{k=1}^{d} \frac{\|x_k - x_k'\|_2^2}{2 l_k^2} \right) \tag{4}$$

where σ and l_k are, respectively, the output standard deviation and a length scale. They are the model hyperparameters and are denoted by the vector $\boldsymbol{\theta} = [\sigma, l_k]$. In terms of function properties, the squared-exponential is related to an infinitely differentiability expected of the modelled function. It is our working assumption that this covariance function is not ideal and Section 4 will be dedicated to discover a covariance function structure appropriate to the (transonic) pressure distribution over a wing. The popularity of the squared-exponential covariance function can also be explained by the few hyperparameters to be identified and the interpretability of those. Indeed, in Eq. (4), the covariance function employs a length scale for each dimension of the design space found through automatic relevance determination [19]. A relatively large length scale corresponds to relatively little variation along the dimension of the modelled function, and vice versa.

The method often used for learning the hyperparameters is based on the evaluation of the likelihood function $p(\mathbf{y}|\boldsymbol{\theta})$. Using the standard form for a multivariate Gaussian distribution, the log-likelihood function is given by

$$\log p(\mathbf{y}|\mathbf{X}, \boldsymbol{\theta}) = -\frac{1}{2} \mathbf{y}^\top \left[k(\mathbf{X}, \mathbf{X}) + \tau^2 \mathbf{I} \right]^{-1} \mathbf{y} - \frac{1}{2} \log \left[k(\mathbf{X}, \mathbf{X}) + \tau^2 \mathbf{I} \right] - \frac{N}{2} \log (2\pi) \tag{5}$$

Gradient-based optimisation algorithms are routinely used to maximise the latter expression. However, it can be seen in Eqs. (2) through (5) that the regression model involves the matrix inversion of $\left[k(\mathbf{X}, \mathbf{X}) + \tau^2 \mathbf{I} \right]$. The number of operations for this matrix inversion scales with N^3 operations. Considering the size of the data sets under investigation, given in Table 1, it leads to scalability limits of the Gaussian process regression and requires additional consideration. While comprehensive reviews of scalable Gaussian processes are available [20], a method based on Stochastic Variational Inference [14,21] was chosen herein to enable the application to the configuration presented in Section 3, i.e. to aircraft wing pressure distributions.

2.2 Fidelity function

To quantify the uncertainty associated with data generated by an information source, we use the fidelity function σ_f as part of the multifidelity framework [11]. It is a representation of the confidence in an information source over the design space and can come from e.g. expert knowledge, past experience and/or empirical data. The fidelity function is defined over the design space $\mathcal{D}$ and relates how the confidence one has in the data varies within that design space. While σ_{GP} accounts for the modelling uncertainty away from the training points, σ_f is an additional term of the same nature quantifying the uncertainty in the available data itself. The resulting total variance is stated as

$$\sigma_t^2 = \sigma_{GP}^2 + \sigma_f^2 \tag{6}$$

and aims to capture both the quality of the Gaussian process model and the expert's confidence in the underlying data. The total variance is then incorporated in each intermediate surrogate model. The posterior standard deviation σ_{GP} is analytically determined by the Gaussian process regression previously described. However, the fidelity function σ_f is challenging to define. Its definition is non-unique, subjective to the user, and depends on several factors such as the method used to obtain the data or the design space considered. Section 5 will an attempt to provide a fidelity function definition based on the test case introduced in Section 3.

2.3 Variance-weighted combination of intermediate surrogate models

As previously presented [11,12,10], a surrogate model is built for every information source, i.e. a Gaussian process regression model is trained from every $\mathbf{f}_i(\mathbf{X}_i)$ produced by the i-th among I information sources. The resulting intermediate posterior mean and standard deviations are denoted $\mu_{GP,i}$ and $\sigma_{GP,i}$, respectively. As defined earlier in Eq. (6), the total variance of the i-th information source is $\sigma_{t,i}^2 = \sigma_{GP,i}^2 + \sigma_{f,i}^2$ where $\sigma_{f,i}$ is the fidelity function defined for the i-th information source. The multifidelity fused estimation of $f(\mathbf{x})$ is computed with a weighted sum of $\mu_{GP,i}$ and $\sigma_{GP,i}$. The weighting [22] to give more importance to high-confidence models is defined by the multifidelity mean estimate and the multifidelity total variance as

$$\overline{\mu}(\mathbf{x}) = \overline{\sigma}^2(\mathbf{x}) \sum_{i=1}^{I} \frac{\mu_{GP,i}(\mathbf{x})}{\sigma_{t,i}^2(\mathbf{x})} \tag{7}$$

$$\overline{\sigma}^2(\mathbf{x}) = \left(\sum_{i=1}^{I} \frac{1}{\sigma_{t,i}^2(\mathbf{x})} \right)^{-1} \tag{8}$$

The approach combines the non-hierarchical multifidelity method to fuse disparate data and the definition of fidelity function to quantify information source uncertainty.

3.0 Civil Aircraft Wing Configuration

3.1 Experimental wind-tunnel test campaign

The work presented here uses data from experiments conducted in the Aircraft Research Association Transonic Wind Tunnel on the RBC12 half wing-fuselage config-

(a) Model mounted on wind tunnel floor   (b) Front, side and top views of geometry
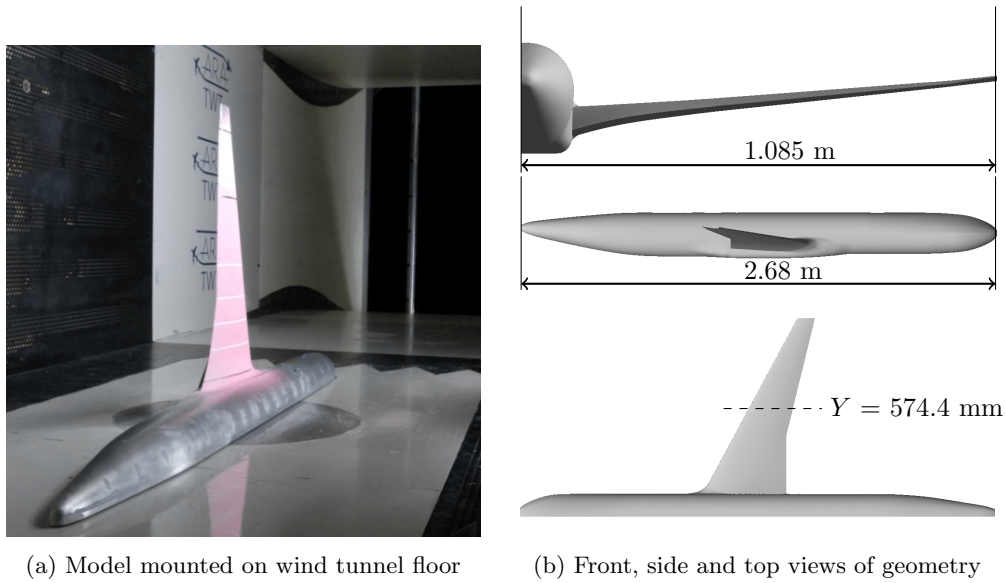
Figure 1: Perspective of installed physical model as well as front, side and top views of computational model.

uration with focus on transonic buffet. Nevertheless, the data considered here are assumed to be steady in pre-buffet conditions. A more detailed description of the experimental study can be found in our previous work[23,24,18]. Figure 1 presents the underlying wing geometry which is representative of a typical 1970s/1980s commercial aircraft design. The wind tunnel model has been scaled down by a factor of 17.5. Its mean aerodynamic chord is 0.279 m with a semi-span of 1.085 m, giving an aspect ratio of 7.78 and a reference area of 0.2959 m^2. The wing is twisted, tapered and swept back with a constant quarter-chord sweep angle of 25°. For visualisation purposes, a dimensionless spanwise coordinate is defined as $\eta = (Y - 0.019)/1.085$, derived for the coordinate Y from which the plinth thickness (0.019 m) is subtracted.

An overview of all available data in this study is shown in Fig. 2 with details discussed next. The chosen flow conditions follow the available data from the previous test campaign including reference Mach numbers between $M = 0.7$ and 0.84, a Reynolds number (with respect to mean aerodynamic chord and reference velocity) of approximately 3.4×10^6 to 3.7×10^6 and angles of attack approximately between $\alpha = -1.2°$ and 8.4°. Herein we focus on pressure features, through the pressure coefficient, over the upper surface of the RBC12 wing. A large number of static pressure taps (chosen as the first data source) were installed on the wing and the fuselage to observe the shock movement and flow development around buffet onset with varying Mach number and angle of attack. A total of 150 static pressure taps are located on the upper surface of the wing. In addition, the second data source is dynamic pressure-sensitive paint (DPSP) recorded with a high-frame-rate imaging system and previously processed to analyse the unsteady behaviour of the shock dynamics with plenty of detail presented in Masini et al.[18]. Such an advanced optical measurement

Table 1: Overview of different data sets.

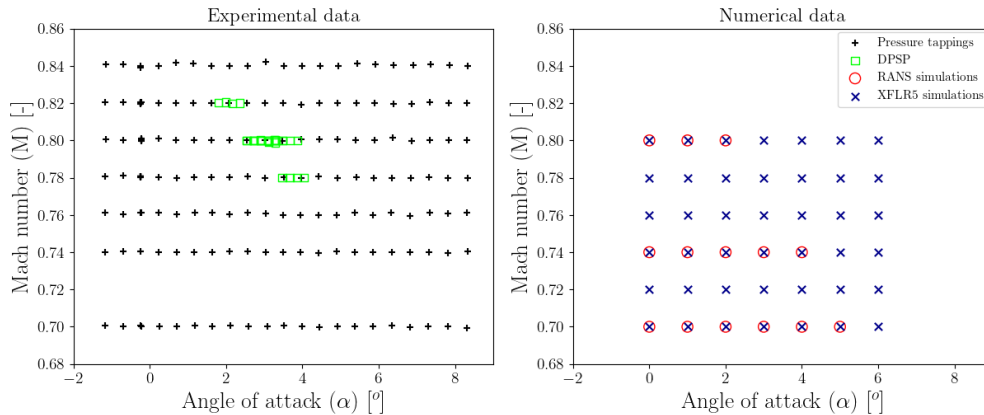| Source	Flow conditions	Spatial coordinates	Dataset size
Pressure tappings	183	150	27,450
DPSP	30	289,215	8,676,450
RANS	14	52,491	734,874
XFLR5	42	900	37,800

Figure 2: Available data according to Mach number and angle of attack.

technique can provide pressure information over a large region of the wing surface, offering a significant advantage over discrete pressure measurements. For instance, the set-up of the previous test campaign resulted in a resolution of 1.3 pixel/mm. The idea is to exploit time-averaged DPSP measurements to benefit from its spatial abundance and to complement scattered static pressure tap data.

3.2 Complementary numerical simulations

Figure 2 (right) shows the experimental conditions at which Reynolds-averaged Navier–Stokes (RANS) and a three-dimensional panel method simulations have been carried out. For RANS computations, the geometry shown in Fig. 1 was reconstructed from the wind tunnel model using a laser-equipped scanner and an unstructured mesh (with approximately 12.2×10^6 vertices) has previously been created following industry best-practice guidelines. The finite volume code TAU [25] was chosen for the simulations. The convective fluxes of the mean flow equations make use of the code's default central scheme with scalar artificial dissipation and those of the turbulence model (chosen to be the negative Spalart–Allmaras model) use a Roe scheme. Gradients for viscous fluxes and source terms use the Green–Gauss relation. To the extent possible, numerical flow conditions have been matched to the available wind tunnel experimental conditions [10].

The wing geometry has been modified to apply panel methods which solve the linear potential flow equations. Rather than only considering the wing planform for the

Table 2: Various basic covariance functions defined in one dimension.

Kernel name	$k(x, x')$	Type of structure
Linear (Lin)	$\sigma^2 (x - c)(x' - c)$	linear functions
Squared-exponential (SE)	$\sigma^2 \exp\left(-\frac{(x-x')^2}{2l^2}\right)$	local variation
Periodic (Per)	$\sigma^2 \exp\left(-\frac{2}{l^2}\sin^2\left(\pi\frac{(x-x')}{p}\right)\right)$	Repeating structure
Rational quadratic (RQ)	$\sigma^2\left(1 + \frac{(x-x')^2}{2\alpha l^2}\right)^{-\alpha}$	multiscale variation
White noise (WN)	$\sigma^2 \delta(x - x')$	uncorrelated noise

discretisation, the model geometry used in XFLR5 accounts for the main geometrical features of the RBC12 wing, such as the aerofoil profile and the twist and dehidral angles (going beyond the usual wing span and local chord lengths to describe the planform). The fuselage has been replaced by a flat wing extension with the same profile as the wing-root profile for modelling purposes. The method implemented in XFLR5[26] has been used to generate the pressure distribution over the model wing computed at the centroid of each panel. Obviously, the potential flow hypothesis lacks accuracy for the transonic Mach numbers (and viscous flow) addressed herein, but the flexibility and execution speed justify its inclusion, while its associated fidelity function will take its inaccuracy into account.

4.0 Data Modelling with Gaussian Processes

4.1 Covariance function structure discovery

A covariance function (also called kernel function) is a positive semi-definite function of input pairs $\mathbf{x}$ and $\mathbf{x}'$[13]. As mentioned earlier, it plays an essential role in the model construction using Gaussian process regression. It includes the properties of the function to be learnt. It can also be seen as a definition of similarity between input points. This aspect is connected to the more general assumption in supervised learning that nearby input points are likely to have a similar output. Therefore, a test point should have a similar output to the nearest training points. However, the flexibility provided by Gaussian process regression is counterbalanced by the necessity to choose this covariance function that best suits the structure of the training data. While the (hyper-) parameters of the covariance function can be obtained by minimising the log-likelihood in Eq. (5), its parametric form must be chosen nevertheless. In addition, combinations of simple covariance functions through addition and multiplication can be used to express a wide range of function structures such as additivity, symmetry, periodicity, interactions between variables, and changepoints[16]. Table 2 defines five basic one-dimensional covariance functions and their associated structure type*. Each of these covariance functions entails assumptions made about the underlying

---

* The output variance σ^2, the offset c, the period p and the parameter α are hyperparameters of their respective covariance functions. The Dirac delta function δ is used for the white noise function.
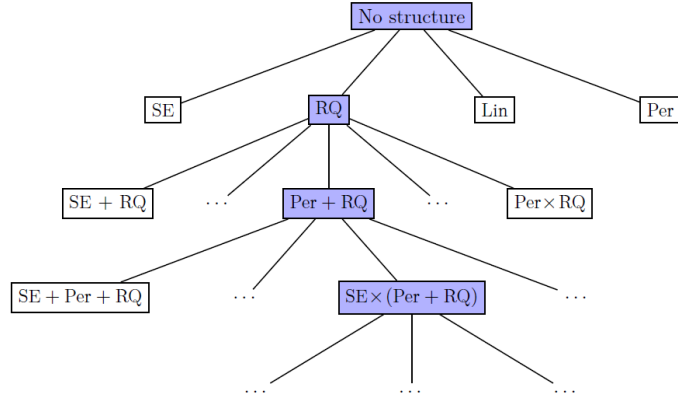
Figure 3: An example of a search tree over covariance functions defined in Table 2. Image reproduced with permission of the author[16].

data. Thus, it is possible to build a custom covariance function with the appropriate properties by combining basic covariance functions with known properties.

For instance, adding a linear covariance function to another covariance function indicates a linear variation in the modelled data. Additivity is a popular assumption, but multiplication can also express interesting properties. Multiplying a covariance function by a linear covariance function illustrates a growing amplitude and by a squared-exponential converts a global variation to a local variation. Another combination of interest is the changepoint (CP) covariance function[17]. It expresses a change between structure types and is defined from two basic covariance functions denoted k_1 and k_2. On a one-dimensional axis, it is defined as

$$k_{CP}^{(k_1,k_2)}(x,x') = s(x)\,k_1(x,x')\,s(x') + \big(1 - s(x)\big)\,k_2(x,x')\,\big(1 - s(x')\big) \qquad (9)$$

with $s(x) = 0.5 + 0.5\tanh(-\xi(x - x_0))$ parameterised by location x_0 of the structure change and steepness ξ indicating how abrupt the change is. A more complete description of the resulting structures and the combination rules is available in Duvenaud[16].

While a wide variety of models can thus be built, typically it is challenging to pick the best covariance function for a given problem. With this in mind, an automatic model construction method was developed[15,16,17] with the objective to search over a space of covariance function structures built by combination of a small number of base expressions. The method is essentially based on two components; (i) a procedure to search the function space and (ii) a procedure using the marginal likelihood to compare models. The space of Gaussian process regression models can be explored using a greedy search[16]. Starting with base covariance functions, the method applies operations such as substitution, multiplication, addition or changepoint to a set of basic covariance functions. At each step, the best model is selected for further operations when proceeding to the next step. The best covariance function at a given step is selected using the Bayesian information criterion (BIC)[27],

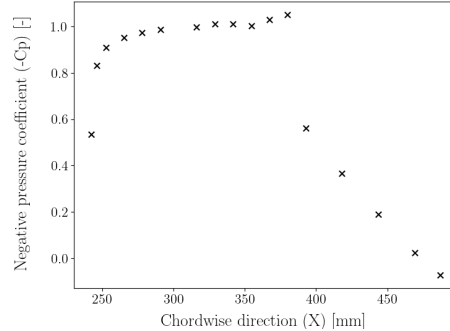$$BIC(\boldsymbol{\theta}) = \log p(\mathbf{y}|\boldsymbol{\theta}) - \tfrac{1}{2}n_\theta \log N \qquad (10)$$

Figure 4: Pressure coefficient on upper wing surface at $\eta = 51\%$.

where n_θ is the number of hyperparameters and N the number of training data. The criterion is based on the marginal likelihood $p(\mathbf{y}|\boldsymbol{\theta})$ penalised by the second term representing the model complexity, i.e. the number of model parameters. The number of steps is chosen by the user and is a trade-off between the model accuracy and its growing complexity. The automatic model construction goals are to explore a large number of models and to discover unexpected structure in training datasets. Source code to perform the search is available online[†] and relies on the GPML toolbox[28].

4.2 One-dimensional results for chordwise pressure distribution

In transonic flow, the presence of shock waves and separation makes it challenging to capture the pressure changes on a wing along the chordwise direction. In the design space considered, the pressure changes in the other dimensions (spanwise direction, Mach number and angle of attack) are smoother and appropriately modelled by standard practices. Thus, we focus the automatic covariance function search on the pressure coefficient along the wing chord on the upper surface. As stated before, the objective is to discover the underlying structure in the training data set and to obtain a covariance function adapted to model transonic wing flow. In terms of the multifidelity data fusion framework, the aim is to improve the construction of the intermediate surrogate models. Figure 4 shows representative training data from pressure tappings at a spanwise location $\eta = 51\%$ ($Y = 574.4$ mm) for case $\{\alpha = 3°,\ M = 0.82\}$, used to demonstrate the automatic structure discovery. As the model search procedure requires training many models, the relatively low number of data points alleviates, for our demonstration purposes, the otherwise significant computational cost.

Only few choices have to be specified to carry out the search for function structure. The initial covariance function is a standard squared-exponential and serves as a first reference for model comparison. The set of covariance functions to be involved in combinations includes the squared-exponential (SE), rational-quadratic (RQ), linear and constant covariance functions. Combinations of those covariance functions are trained on the reference dataset and are compared in turn to advance the search. The

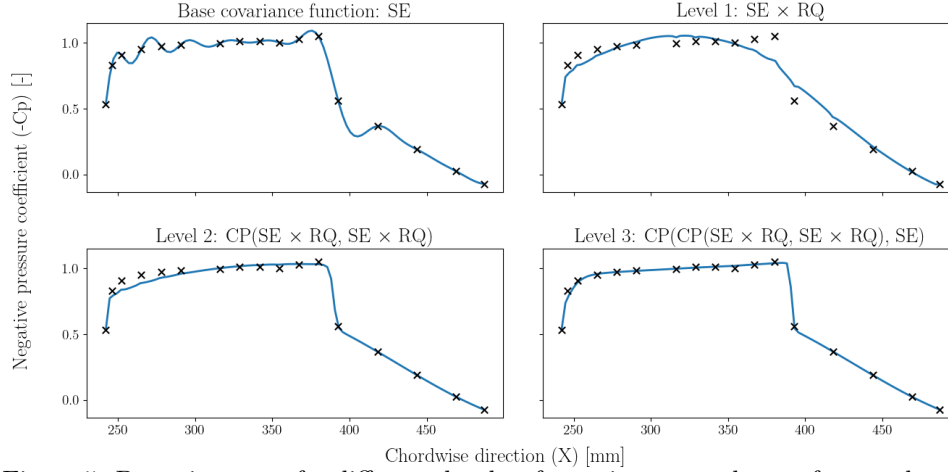[†] http://www.github.com/jamesrobertlloyd/gp-structure-search

Figure 5: Posterior mean for different depths of covariance search on reference dataset.

best model amongst many at each level, judged from the BIC as given in Eq. (10), for a four-level search with increasing complexity are presented in Fig. 5. For clarity and because the main interest is the modelling aspect, the illustrations are limited to the posterior mean of each model.

It is observed that in the case of noise-free regression, the model with the base covariance function (level 0) is overfitting the data and presents some visually inaccurate oscillation. It is due to the characteristics of the squared-exponential to model smooth variations depending on the length scale. Some improvements are noted at level 1 of the search by multiplying the base covariance function by a rational-quadratic. The latter incorporates multiscale variation in the data. The multiplication by the squared-exponential involves removing long range correlations from the model as the function tends to zero with the increase of $(x - x')^2$. However, it can be seen that the shock is poorly captured by the model. While the overfitting is less prominent, the posterior mean is too smooth at the location of the shock wave. Level 2 introduces the changepoint function which is more accurate to represent the variation of the pressure coefficient around the shock discontinuity. Indeed, the changepoint represents a change in terms of structure in the data and allows the switch between two covariance functions with the expressions of level 1. Those two multiplications of covariance functions, SE and RQ, have consequently different hyperparameter values. Level-2 posterior mean underestimates the pressure coefficient around the leading edge. This issue is overcome in level 3 where a new change point composes the covariance function of level 2 with a squared-exponential at the location near the leading edge. The model corresponding to level 3 appear to describe the evolution of the data well. The shock-related changepoint around $X = 390$ mm seems arbitrary in the sense that it is not certain that the location of the shock wave is exactly captured. Additional, more refined data information would help determining the exact behaviour of the pressure coefficient around this location. Overall, the model improves with each level, but it is important to recall that also the complexity of the model increases, so there are more
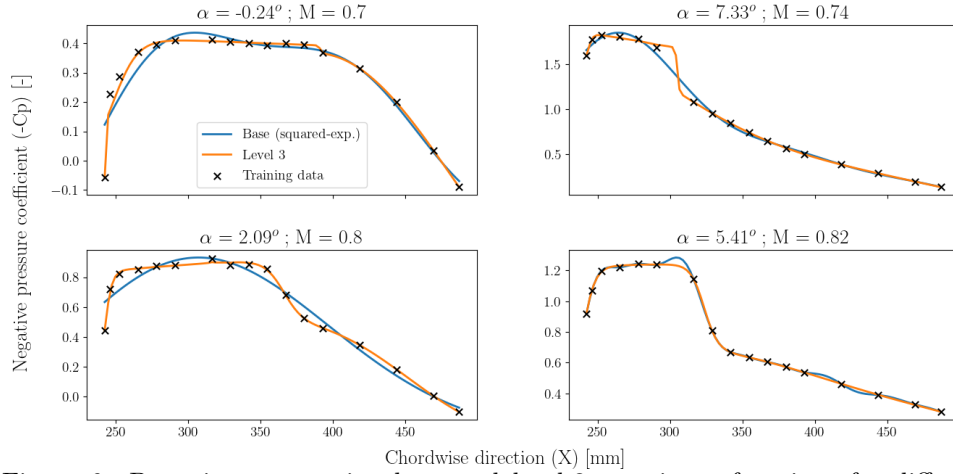
Figure 6: Posterior mean using base and level-3 covariance functions for different experimental conditions.

hyperparameters to determine, which can be problematic, and this is accounted for in the BIC with the penalty term.

As this best level-3 model structure has been obtained for a particular experimental condition, it is important to query how the model generalises to other conditions where the pressure evolution will be different. Figure 6 shows a comparison of the posterior mean between a standard squared-exponential (base covariance function) and the best level-3 covariance function structure (identified in Fig. 5) for four unseen pairs of angle of attack and Mach number. For case $\{\alpha = –0.24°, M = 0.7\}$, the behaviour of both model structures is similar as the evolution of the pressure coefficient is smoother, with the exception of the leading edge where the base covariance function does not capture the variations well. This confirms the importance for the covariance function to have a changepoint at this location. The observations are similar for the other cases, $\{\alpha = 2.09°, M = 0.8\}$ and $\{\alpha = 5.41°, M = 0.82\}$, with the variations clearly better captured by the level-3 covariance function. An interesting result is that the changepoint location, i.e. the abrupt pressure change due to the shock, is well identified during the model training. Indeed, it is a model hyperparameter and is therefore optimised during training. The difference between the two covariance functions is less straightforward for the final case $\{\alpha = 7.33°, M = 0.74\}$. While the level-3 model is better at the leading edge, the behaviour at streamwise location between approximately $X = 290$ mm and 325 mm is uncertain for both covariance functions. The base covariance function underfits the data at this location and the more complex model predicts a steep change in the middle of the two known data. Additional pressure-tap data would help to discern the correct evolution better.

It can be concluded that the covariance function identified during the automatic model search using an arbitrarily selected flow condition generalises well to other experimental conditions of the design space and provides a satisfying model for transonic flow conditions. The key insight of this study is the powerful use of changepoints to

incorporate the steep variations when shock waves are involved. While these results are currently limited to a one-dimensional application and also require more scrutiny, in future work we will explore the extension to multidimensional regression in order to integrate them into the multidimensional multifidelity data fusion framework.

5.0 Fidelity Function Definition

In engineering design, an important and persistent challenge is to know always to what extent one can trust the available data. Several factors must be taken into account when quantifying this confidence. Aerodynamic studies rely to a great extent on simulations and wind tunnel testing, which are both subject to multiple sources of uncertainty. In the context of multifidelity data fusion, the uncertainty quantification of an information source provides both the confidence in data obtained from it and the relative accuracy with respect to other information sources at that point in the design space. Indeed, the multifidelity approach considered herein is non-hierarchical and the uncertainty has to be defined independently in the design space for each information source. It is represented by the fidelity function defined in Eq. (6). Previously, the data fusion framework has been applied to the RBC12 configuration, assuming the four fidelity functions to be constant in the design space for demonstration purposes while still representing the desired influence of each of the four information sources[10]. The objective is now to discuss a better grounded definition of the respective fidelity functions defined on the input space. We limit the discussion to four dimensions herein, specifically Mach number and angle of attack, and the spatial coordinates (X, Y) in stream- and spanwise directions, respectively.

Figure 2 shows the experimental flow conditions tested in the Aircraft Research Association Transonic Wind Tunnel. Wind tunnel conditions aim to reproduce an environment similar to those of the vehicle's real flight conditions. There are several factors why the real flight conditions cannot be reproduced perfectly. Consequently, many wind tunnel corrections are applied by the test engineers to account e.g. for blockage effects, buoyancy effects or flow angle divergence[18,23]. In addition, measurement errors can affect the data from the pressure sensor to the acquisition system. Each wind tunnel test is unique and will lead to different uncertainties and calibrations, but a reasonable estimate of experimental noise and error can be given. It is represented herein by a constant value in the design space which means that the confidence on the data does not vary with respect to the dimensions of the design space. For pressure-tap data, the confidence in the absolute pressure measurement established by experimentalists is expressed in terms of the fidelity function $\sigma^2_{f,\text{Tap}}$. Without going into detail concerning the DPSP data acquisition (for more information see Masini et al.[18]), the local pressure values obtained on the wing surface result from the varying fluorescent intensity of the paint. It requires the calibration with scattered pressure-tap data and is hence subject to the same assumptions and uncertainties mentioned before. However, thermal effects affect the paint response and lead to a lower confidence in the DPSP data. The use of DPSP is justified by a high spatial resolution, but the resulting data is believed to be physically less accurate compared with taps. It is important to recall that the values chosen for the application below are from expert opinion and case-dependent and are therefore not unique.
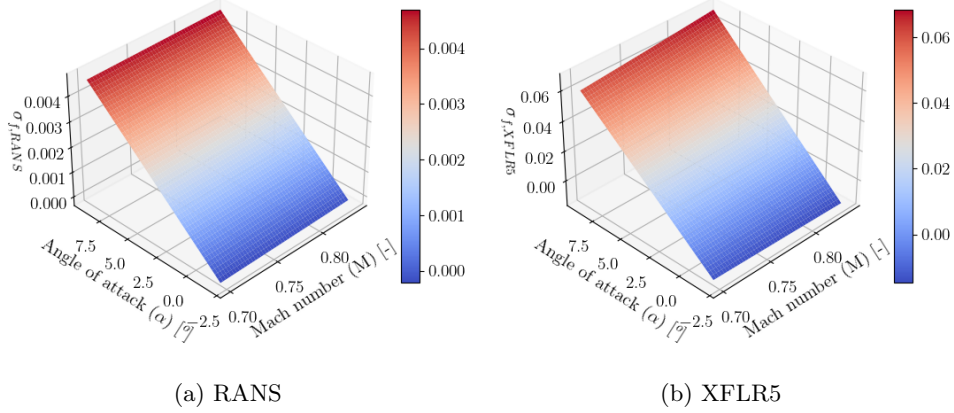
(a) RANS (b) XFLR5

Figure 7: Fidelity function evolution for RANS and XFLR5 information sources over $(M, \alpha) \in [0.7, 0.84] \times [-2°, 9°] \subset \mathcal{D}$

Defining the fidelity function for numerical data sources is different. It is established in the literature that uncertainty in numerical simulations can be divided in two types; numerical and modelling uncertainties[29,30,31]. The former is due to the nature of the information source itself, i.e. the use of numerical methods to solve the problem, and results from e.g. discretisation, iterative convergence and round-off errors. It can be represented by a constant in the design space but it is difficult to quantify exactly. The latter is associated with physical approximation errors in the modelling of the fluid problem. For instance, turbulent flow is normally approximated by the governing RANS equations and choice of turbulence model. It can also be linked to the approximations made to represent the actual geometry in the simulation. Modelling uncertainties vary with flow conditions because the leading physical phenomena can change. For instance, shock related phenomena are more important at higher Mach numbers or the boundary layer separation occurs at a certain angle of attack.

The fidelity function for the first numerical information source can be written as the sum of these two terms, $\sigma_{f,\mathrm{RANS}}(\mathcal{D}) = \sigma_{f,\mathrm{numerical}} + \sigma_{f,\mathrm{modelling}}(M, \alpha)$. An expression is derived from a validation step with experimental pressure-tap data (considered as the most reliable source) and proposed here (for 99.7% confidence interval),

$$3\sigma_{f,\mathrm{RANS}} = 0.008 \left(1 + M + 0.5\alpha\right) \tag{11}$$

It is defined for any $(M, \alpha) \in [0.7, 0.84] \times [-2°, 9°] \subset \mathcal{D}$ and aims to describe the confidence change over the design space, particularly with the experimental conditions. Concerning the second numerical information source, the fidelity function formulation is similarly decomposed. However, as stated in Section 3, the potential flow hypothesis is not appropriate for the experimental conditions considered. Also, the model geometry has been simplified to match XFLR5 requirements. This leads to higher values of the fidelity function (lower confidence in the data) which increase with the respective
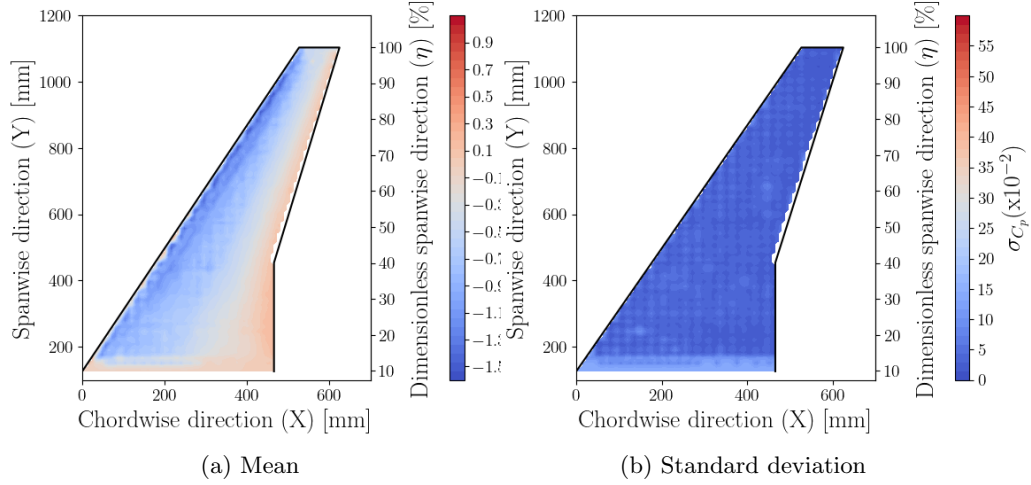
(a) Mean

(b) Standard deviation

Figure 8: Multifidelity surrogate model predicted at $\alpha = 3.0°$ and $M = 0.8$

increase of the experimental conditions. The following expression is suggested,

$$3\sigma_{f,\mathrm{XFLR5}} = 0.01\left(1 + e^{0.5\alpha + 2M}\right) \tag{12}$$

The evolution of these fidelity functions is plotted in Fig. 7. It can be observed that the values of fidelity function attributed to the RANS data are lower than the XFLR5 ones, which accounts for the lack confidence in the latter. The definitions proposed in Eqs. (11) and (12) are examples and intended to demonstrate the definition of a suitable function varying over the design space as a result of the confidence that is placed in the information source. Other definitions are possible to quantify the uncertainty associated with numerical simulations.

The fidelity functions defined for the four information sources are applied in the data fusion framework on the four-dimensional design space. The multifidelity posterior mean and standard deviation of the surface pressure coefficient for angle of attack $\alpha = 3.0°$ and Mach number $M = 0.8$ are plotted in Fig. 8. This set of flow parameters is chosen as it is representative of the design of experiments represented in Fig. 2. As previously noted[10], the resulting multifidelity posterior mean has a contour with physically coherent shape. It is thus shown that it is possible to integrate expert knowledge into the multifidelity data fusion framework through the fidelity function definition. As the total standard deviation influences the extent to which an information is taken into account in the final model, the fidelity function directly allows the user to employ their domain-specific knowledge of the information source to obtain a physically consistent model with a quantified uncertainty.

6.0 Conclusions

A multifidelity data fusion framework previously introduced and based on a variance-weighted combination of intermediate Gaussian process models has been further scrutinised herein. It has been applied to a design space with up to four dimensions with

available data describing civil aircraft wing pressure distributions obtained from experimental and computational methods. The focus has been on the two important aspects of building the intermediate models, specifically the covariance function, and defining a fidelity function. Regarding the first point, an automatic model search process has been applied to find a covariance function that best fits the evolution of the pressure coefficient in the streamwise direction, which has led to a more complex covariance function composed of combinations of simple expressions. In particular, the use of changepoints has been beneficial in capturing abrupt streamwise pressure changes related to shock waves, characteristic of transonic flow. Future work will aim to adapt the approach to multidimensional problems. The second point explored non-exhaustive examples of defining the fidelity function for the test case considered here. A distinction has been made between experimental and numerical information sources. It has been shown that expert opinion can be embedded into the data fusion process independently for each information source. This reinforces the interest in a non-hierarchical multifidelity data fusion framework.

Acknowledgements

References

1. D.G. Krige. A statistical approach to some basic mine valuation problems on the witwatersrand. *Journal of the Southern African Institute of Mining and Metallurgy*, 52(6):119–139, 1951.

2. D.E. Myers. Matrix formulation of co-kriging. *Journal of the International Association for Mathematical Geology*, 14(3):249–257, 1982.

3. Y. Kuya, K. Takeda, X. Zhang, and A.I.J. Forrester. Multifidelity Surrogate Modeling of Experimental and Computational Aerodynamic Data Sets. *AIAA Journal*, 49(2):289–298, 2011.

4. A.I.J Forrester, A. Sóbester, and A.J. Keane. Multi-fidelity optimization via surrogate modelling. *Proceedings of the Royal Society A: Mathematical, Physical and Engineering Sciences*, 463(2088):3251–3269, 2007.

5. S. Timme and K. J. Badcock. Transonic Aeroelastic Instability Searches Using Sampling and Aerodynamic Model Hierarchy. *AIAA Journal*, 49(6):1191–1201, 2011.

6. A. J. Keane. Wing Optimization Using Design of Experiment, Response Surface, and Data Fusion Methods. *Journal of Aircraft*, 40(4):741–750, 2003.

7. X. Wen, Z. Li, D. Peng, W. Zhou, and Y. Liu. Missing data recovery using data fusion of incomplete complementary data sets: A particle image velocimetry application. *Physics of Fluids*, 31(2):025105, 2019.

8. S.A. Renganathan, K. Harada, and D.N. Mavris. Aerodynamic Data Fusion Toward the Digital Twin Paradigm. *AIAA Journal*, 58(9):3902–3918, 2020.

9. A. Bertram, P. Bekemeyer, and M. Held. Fusing Distributed Aerodynamic Data Using Bayesian Gappy Proper Orthogonal Decomposition. In *AIAA AVIATION 2021 FORUM*, VIRTUAL EVENT, 2021.

10. M. Anhichem, S. Timme, J. Castagna, A. Peace, and M. Maina. Multifidelity Data Fusion Applied to Aircraft Wing Pressure Distribution. In *AIAA AVIATION 2022 Forum*, Chicago, IL, 2022.

11. R. Lam, D.L. Allaire, and K.E. Willcox. Multifidelity Optimization using Statistical Surrogate Modeling for Non-Hierarchical Information Sources. In *56th AIAA/ASCE/AHS/ASC Structures, Structural Dynamics, and Materials Conference*, Kissimmee, FL, 2015.

12. A. Feldstein, D. Lazzara, N. Princen, and K. Willcox. Multifidelity Data Fusion: Application to Blended-Wing-Body Multidisciplinary Analysis Under Uncertainty. *AIAA Journal*, 58(2):889–906, 2020.

13. C.E. Rasmussen and C.K.I. Williams. *Gaussian Processes for Machine Learning*. Adaptive Computation and Machine Learning. MIT Press, Cambridge, MA, January 2006.

14. J. Hensman, N. Fusi, and N.D. Lawrence. Gaussian processes for big data. In *Proceedings of the Twenty-Ninth Conference on Uncertainty in Artificial Intelligence*, UAI'13, page 282–290, Arlington, VA, 2013. AUAI Press.

15. D. Duvenaud, J.R. Lloyd, R. Grosse, J.B. Tenenbaum, and Z. Ghahramani. Structure discovery in nonparametric regression through compositional kernel search, 2013.

16. D. Duvenaud. *Automatic model construction with Gaussian processes (Doctoral thesis)*. PhD thesis, 2014.

17. J.R. Lloyd, D. Duvenaud, R. Grosse, J.B. Tenenbaum, and Z. Ghahramani. Automatic construction and natural-language description of nonparametric regression models, 2014.

18. L. Masini, S. Timme, and A.J. Peace. Analysis of a civil aircraft wing transonic shock buffet experiment. *Journal of Fluid Mechanics*, 884:A1, 2020.

19. K. Liu, Y. Li, X. Hu, M. Lucu, and W.D. Widanage. Gaussian process regression with automatic relevance determination kernel for calendar aging prediction of lithium-ion batteries. *IEEE Transactions on Industrial Informatics*, 16(6):3767–3777, 2020.

20. H. Liu, Y.-S. Ong, X. Shen, and J. Cai. When Gaussian Process Meets Big Data: A Review of Scalable GPs. *IEEE Transactions on Neural Networks and Learning Systems*, 31(11):4405–4423, 2020.

21. J. Hensman, A. Matthews, and Z. Ghahramani. Scalable variational gaussian process classification. In *Artificial Intelligence and Statistics*, pages 351–360. PMLR, 2015.

22. R.L. Winkler. Combining Probability Distributions from Dependent Information Sources. *Management Science*, 27(4):479–488, 1981.

23. S. Lawson, D. Greenwell, and M.K. Quinn. Characterisation of Buffet on a Civil Aircraft Wing. In *54th AIAA Aerospace Sciences Meeting*, San Diego, CA, 2016. AIAA 2016-1309.

24. F. Sartor and S. Timme. Delayed detached–eddy simulation of shock buffet on half wing–body configuration. *AIAA Journal*, 55(4):1230–1240, 2017.

25. D. Schwamborn, T. Gerhold, and R. Heinrich. The DLR TAU-code: Recent applications in research and industry. In *ECCOMAS CFD 2006 Conference*, 2006.

26. B. Maskew. A computer program for calculating nonlinear aerodynamic characteristics of arbitrary configurations. In *Program VSAERO Theory Document*, NASA Contractor Report 4023. NASA, Ames Research Center, 1987.

27. G. Schwarz. Estimating the Dimension of a Model. *The Annals of Statistics*, 6 (2), 1978.

28. C.E. Rasmussen and H. Nickisch. Gaussian processes for machine learning (gpml) toolbox. *Journal of Machine Learning Research*, 11(100):3011–3015, 2010. URL http://jmlr.org/papers/v11/rasmussen10a.html.

29. H. W. Coleman and F. Stern. Uncertainties and CFD Code Validation. *Journal of Fluids Engineering*, 119(4):795–803, 1997.

30. W.L. Oberkampf, K.V. Diegert, K.F. Alvin, and B. Rutherford. Uncertainty and error in computational simulations. 1997.

31. D. Bestion, A. de Crecy, F. Moretti, R. Camy, A. Barthet, S. Bellet, J. L. Munoz Cobo, A. Badillo, B. Niceno, P. Hedberg, M. Scheuerer, and A. Nickolaeva. Review of uncertainty methods for CFD application to nuclear reactor thermalhydraulics. In *NUTHOS 11- The 11th International Topical Meeting on Nuclear Reactor Thermal Hydraulics, Operation and Safety*, Gyeongju, South Korea, 2016.